Ballistic ΔS=2 Intersystem Crossing in a Cobalt Cubane Following Ligand-Field Excitation Probed by Extreme Ultraviolet Spectroscopy

Yusef Shari'ati[a] and Josh Vura-Weis[a]

Femtosecond $M_{2,3}$-edge X-ray absorption near-edge structure (XANES) spectroscopy is used to probe the excited-state dynamics of the cobalt cubane $[Co^{III}_4O_4](OAc)_4(py)_4$ (OAc = acetate, py = pyridine), a model for water oxidation catalysts. After ligand-field excitation, intersystem crossing to a metal-centered quintet occurs in 38 fs. 30% of the hot quintet undergoes ballistic back-ISC directly to the singlet ground stat, with the remainder relaxing to a long-lived triplet.

The realization of renewable solar fuels on a global scale requires the development of earth-abundant water oxidation catalysts. The tetrametallic oxo-cluster, $[Co^{III}_4O_4](OAc)_4(py)_4$ (OAc = acetate, py = pyridine), henceforth "Co_4O_4", is a promising molecular compound that has attracted significant interest due to its provocative "cubane" structure which bears a strong resemblance to the active core of the oxygen-evolving complex (OEC) of photosystem II in plants. Co_4O_4 (shown in Figure 1A) also exhibits water oxidation activity in several homogeneous photocatalytic systems,[1–3] as well as in heterogeneous studies where it has been incorporated into photoanodes of TiO_2, Fe_2O_3, and $BiVO_4$.[4–8] Under the high intensity irradiation conditions of photocatalysis, Co_4O_4 excited states may be populated either through direct absorption or via energy transfer from a photosensitizer.

The excited-state dynamics of Co(III) complexes have received fairly little study, especially compared to their isoelectronic Fe(II) counterparts.[9,10] Optical transient absorption spectroscopy of amine-coordinated Co(III) complexes such as Co(ethylenediamine)$_3^{3+}$ indicate picosecond relaxation to quintet metal-centered (^{5}MC) states after ligand-to-metal charge transfer excitation, whereas Co(acac)$_3$ was proposed to relax to triplet MC states (^{3}MC) in 10-20 fs followed by vibrational relaxation on the triplet surface.[11,12]

In this work, we use femtosecond M-edge X-ray Absorption Near Edge Structure (XANES) spectroscopy to measure a cascade of intersystem crossing events in Co_4O_4 after ligand-field excitation, including a surprising efficient ΔS=2 crossing between the hot $^5T_2$ state and the $^1A_1$ ground state. M-edge XANES probes *3p→3d* transitions in the extreme ultraviolet spectral region (40-100 eV) and is a sensitive reporter of spin state, oxidation state, and ligand field symmetry. This technique been previously used to examine excited state dynamics, including ISC, in metal oxides,[13–15] semiconductors,[16–19] and molecular complexes.[20–22]

Co_4O_4 consists of four low-spin d^6 Co^{3+} atoms, each of which is in an approximately octahedral ligand field. The UV-Visible spectrum of Co_4O_4 (Figure S1) exhibits three features in the 300-1000 nm range. A prominent feature at 364 nm has been assigned as a $O^{2-}(2p)\rightarrow Co^{3+}(e_g)$ ligand-to-metal-charge-transfer (LMCT) band based on its strength (~10^4 L mol^{-1} cm^{-1}) and by comparison to other compounds bearing Co-O bonds.[14,23,24] The two lower energy features (451 nm and 646 nm) are consistent with *d-d* transitions, which in the limit of O_h symmetry correspond to $^1A_1\rightarrow{}^1T_2$ and $^1A_1\rightarrow{}^1T_1$ transitions. Analysis of the d^6 Tanabe-Sugano (TS) diagram yields a ligand field splitting 10Dq of 2.1 eV and predicts $^3T_{1g}$ as the lowest energy excited state (see supplemental information). This 10Dq is consistent with published values for octahedral Co^{3+} complexes bearing aquo, carbonato, or oxalato ligands which present an electronic environment similar to that of Co_4O_4.[25] Rigorously speaking, cobalt sites in Co_4O_4 are not of O_h symmetry due to the lone axial pyridine. Tetragonal distortion likely contributes to the relatively high molar absorptivity (~500 L mol^{-1} cm^{-1}) of the *d-d* transitions.

M-edge XANES spectra of Co_4O_4 were acquired from thin film samples of the complex deposited upon polymer membranes.[26] The extreme ultraviolet probe continuum was produced by high-harmonic generation in a tabletop instrument using a Ti:sapphire driving laser (800 nm, 4mJ, 35 fs, 1 kHz) focused into a ~100 torr neon gas cell.[27] Time-resolved experiments utilized the focused ~2.5 mJ/cm^2 550 nm pump output of a noncollinear optical parametric amplifier driven from a 0.65 mJ portion of the same laser. Absolute time zero was determined and corrected for by periodic measurement of the instrument-response limited onset of Fe_2O_3 signal after 550 nm excitation,[13] with the instrument response function (IRF) found to be 48 fs FWHM.

The M-edge XANES spectrum of Co_4O_4 is shown in Figure 1B. It exhibits a three-peaked structure with features at 64.2, 66.2, and 72.3 eV. Ligand field multiplet (LFM) simulations of low-spin Co_4O_4 were performed using CTM4XAS, as detailed in the supplemental information. The simulations reproduce the position of the three features, though the height of the middle peak is overestimated.

The transient M-edge XANES response after *d-d* excitation at 550 nm is shown in Figure 2A, with spectral slices at selected delay times in Figure 2B. A short-lived signal is apparent at the

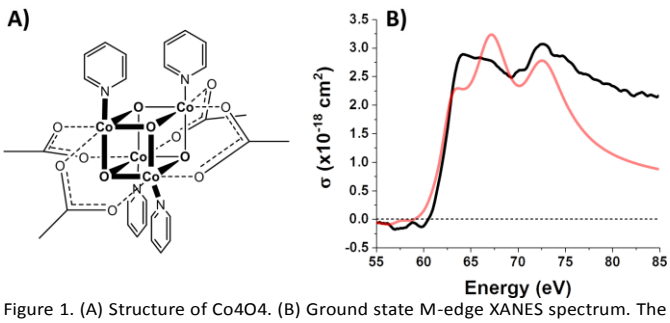

Figure 1. (A) Structure of Co4O4. (B) Ground state M-edge XANES spectrum. The ligand field multiplet (LFM) simulation is shown in red.

earliest delay times and exhibits two sharp peaks at 61.6 and 64.6 eV, with weak ground state bleaches at energies below 58 eV and above 71.4 eV. This initial spectrum transforms within tens of femtoseconds to a longer-lived spectrum characterized by a strong absorption at 62.8 eV, a smaller secondary peak at 65.6 eV, and the same ground state bleaches as the initial signal. The signal subsequently undergoes a loss in intensity from 110 to 160 fs without change in shape. The spectral shape begins to evolve again by 1 ps; the main 62.8 eV feature diminishes further while the bleach near 72.5 eV has instead become positive. Finally, the signal decays away over hundreds of picoseconds completely disappearing by 3 ns.

Figure 3A shows the time traces at 61.6 and 62.8 eV corresponding to the maxima of the initial short-lived spectrum and its immediate successor. The rapidity of the spectral evolution at early times suggest a process faster than is physically reasonable for exponential (first-order) kinetics. These dynamics are better described by coherent motion on the potential energy surface (PES) where the population of excited molecules follows a ballistic trajectory towards a curve crossing.[28,29] Such a ballistic model was implemented with transit time constants ω_1 and ω_2 after which the entire population, bound by the 48 fs IRF, moves into the subsequent state. The transient data were subjected to global analysis in a four-state rate model according to $A \overset{\omega_1}{\rightarrow} B \overset{\omega_2}{\rightarrow} C \overset{t_3}{\rightarrow} D \overset{t_4}{\rightarrow} GS$.

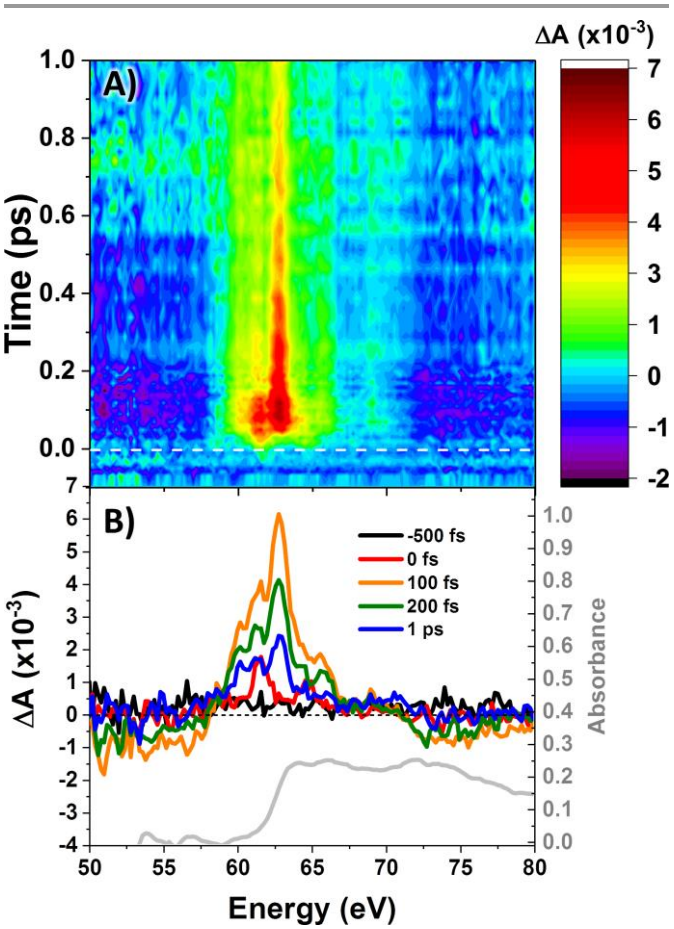

Figure 2. (A) Contour plot of time-resolved M-edge XANES spectra. Time zero is indicated in the dashed white line. (B) Selected spectral slices in the first picosecond with the ground state Co_4O_4 spectrum in grey for comparison.

Extracted from the model are the transit times ω_1 = 38 fs, ω_2 = 94 fs, and exponential time constants τ_3 = 794 fs, and τ_4 = 83 ps. This model yielded the component spectra in Figure 3B.

Photoexcitation into the $^1T_1$ state populates antibonding e_g orbitals, induces bond expansion, and propels the system towards an intersection with nearby low-lying triplet and quintet states, any of which are plausible candidates for the singlet's relaxation products. LFM simulated difference spectra of these states are shown in Figure 4A. The simulated $^1T_1$ difference spectrum exhibits two positive features near 60 and 65 eV with a negative feature between them near 62.5 eV, being a qualitative match to Component A in Figure 3B. Component A decays sequentially into Components B and C, whose extracted difference spectra are nearly identical in shape (see Figure 3B, and normalized in Figure S6B) and likely represent the same electronic state. These are characterized by a strong positive absorption at 62.8 eV, two positive shoulders at 65.6 eV and 69.0 eV, and a broad bleach at energies greater than 71.4 eV. A broad bleach also occurs prior to the edge near 57 eV. These features are reproduced in the simulated quintet $^5T_2$ difference spectrum in Figure 4A, whereas the simulated triplets in contrast are a poor match. This suggests that the singlet excited state undergoes rapid two-electron intersystem crossing to the quintet state. If an intermediate triplet state were involved it would have to be extremely short-lived (<30 fs). Finally, the weak transient signal of Component D emerges. Relative to C, Component D bears a broadened positive absorption near 62.8 eV and the 72.5 eV bleach has become a positive excited state absorption – features characteristic of the $^3T_1$ triplet simulation.

Further corroboration of these assignment is achieved by comparison with Fe(II) spin-crossover complexes,[22,28,30,31] which

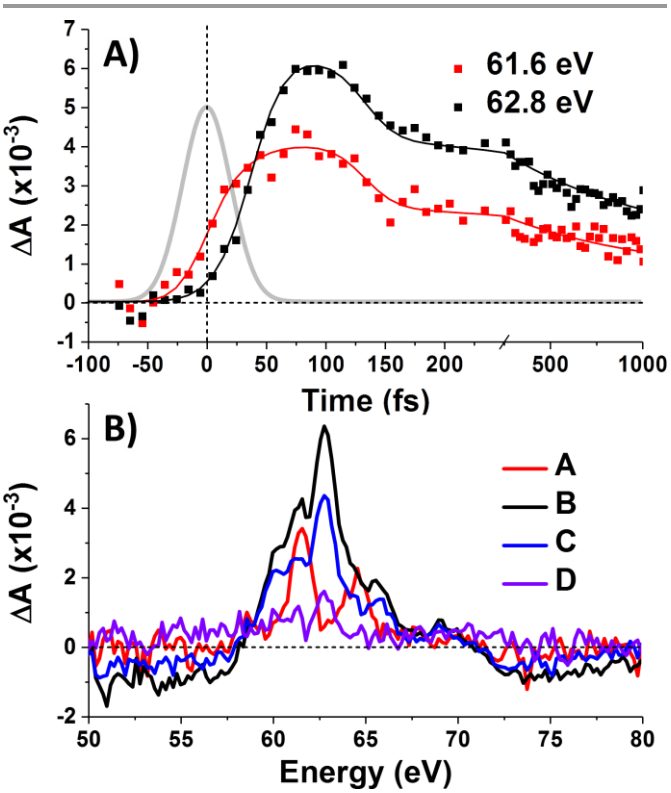

Figure 3. (A) Time traces (data points) with fits (solid lines). The 48 fs instrument response function is plotted in grey. (B) Component spectra.

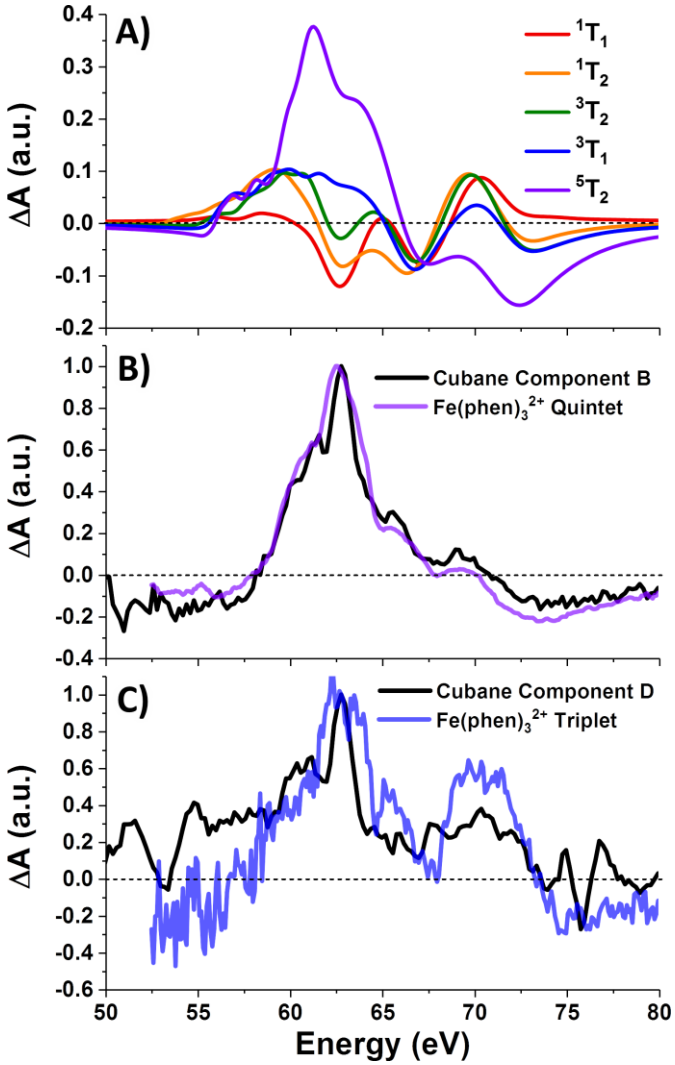

Figure 4. (A) LFM simulations of cubane excited states, and (B) normalized quintet difference spectra of $Fe(phen)_3^{2+}$ (from ref. 22) compared with that of cubane component B, and (C) triplet intermediate spectrum (ibid.) compared with cubane component D. $Fe(phen)_3^{2+}$ spectra have been blue-shifted 5.5 eV, and a 5-point Savitzky-Golay smooth applied to cubane component D.

are isoelectronic to the d^6 metal centers in the cubane. A recent transient $M_{2,3}$-edge XANES study found that $Fe(phen)_3^{2+}$ (phen = *o*-phenanthroline), after pumping into its metal-to-ligand charge transfer (MLCT) band at 535 nm, relaxes to an intermediate $^3T_1$ state and then into a metastable $^5T_2$ state.[22] The difference spectra associated with these two states are reproduced in Figure 4B-C along with the component spectra B and D of cubane. With a +5.5 eV shift applied to the $Fe(phen)_3^{2+}$ data to account for the increased *3p* binding energy of cobalt, the spectra are a good match in the case of the triplet, and essentially superimposable for the quintet.

The picture that emerges (illustrated schematically in Figure 5) is consistent with the state orderings predicted from both the TS diagram and DFT calculations (see SI). After ligand-field excitation into the singlet, the system rapidly (38 fs) follows a ballistic trajectory into the quintet manifold. Descending on the quintet surface, it encounters a crossing with the singlet GS after ~130 fs and loses 30% of its population there. The remaining 70% cools on the quintet surface, then converts into the lowest energy triplet over several picoseconds. The LFM simulations in Figure 4A predict that the triplet transient should be ~25% the strength of the quintet, which is seen here experimentally. If the calculations underestimate this ratio, then the loss in intensity accompanying $^5T_2 \rightarrow {}^3T_1$ conversion can be explained by an additional parallel exponential decay pathway to the GS. Finally, the metastable triplet relaxes with exponential kinetics back to the ground state in 83 ps.

The rapid ΔS=2 intersystem crossing from the $^1T_1$ state to the $^5T_2$ state may be understood in the context of extensive research on Fe(II) chromophores. After ^{1}MLCT excitation, intersystem crossing to the ^{3}MLCT and internal conversion to a ^3T state occur in 100-150 fs, followed by $^3T \rightarrow {}^5T$ ISC in ~50 fs. These inverted kinetics led to early controversy[30,32] over the presence of the ^3T state, but the brief occupation of this state was later confirmed using spin-sensitive core-level spectroscopy.[22,28] This model was supported by theoretical work which rationalized this possibility by re-evaluating the effective spin-orbit coupling between those states—finding it highly geometry dependent—and showed the importance of molecular vibrations on the magnitude of spin-vibronic coupling.[33–36] Predicted ISC rates are often over 10^{13} s^{-1}, with the doublet-to-quartet process in Fe-Co Prussian-blue analogues calculated to be as little as 20 fs.[37] Intersystem crossing between metal-centered states with ΔS=1 occurs with essentially 100% quantum yield at the crossing point between electronic PESs, as shown by work combining x-ray emission spectroscopy and x-ray scattering.[28]

In the present work, the relatively slow ^{3}MLCT$\rightarrow {}^3T$ step is avoided by directly exciting the $^1T_2$ *d-d* state. Similarly, in an Fe(II) complex, *d-d* excitation was shown to populate the ^5T state in as little as 70 fs, leading to enhanced 80 cm^{-1} coherent oscillations on the quintet surface due to lack of dephasing in the MLCT state.[31] The 635 cm^{-1} IR band of Co_4O_4 has been assigned to Co-O stretching vibrations involving the $Co_3(\mu_3\text{-}O)$ core, with a short (53 fs) period.[38] This frequency is significantly higher than the ~250 cm^{-1} (~133 fs) mode in most Fe-N_6 complexes and is likely the primary determinant for the consequentially rapid 38 fs ΔS=2 process in Co_4O_4. Hence, the limiting factor is not the magnitude of spin-orbit coupling matrix element, but rather the frequency of M-L stretching modes on the PESs.

The most surprising result of this study is the high (30%) yield of back-ISC upon a single crossing of the $^5T_2/^1$GS surfaces, as shown by the IRF-limited drop in the intensity of the $^5T_2$ spectrum at 130 fs. While the ΔS=2 forward-ISC could be rationalized as two subsequent ΔS=1 processes that are unresolved given the time resolution of this study, there is no intermediate triplet in this portion of the quintet PES. To first order, the spin-orbit coupling matrix element for the double spin-flip is zero. However, second-order SOC can lead to significant coupling between singlet and quintet states, and mediates the back-ISC from the $^5T_2$ state in molecules such as $Fe(bpy)_3^{2+}$, on ~ns timescales.[39] The second-order coupling is especially significant in the presence of large distortions from the equilibrium geometry as are found in vibrationally hot

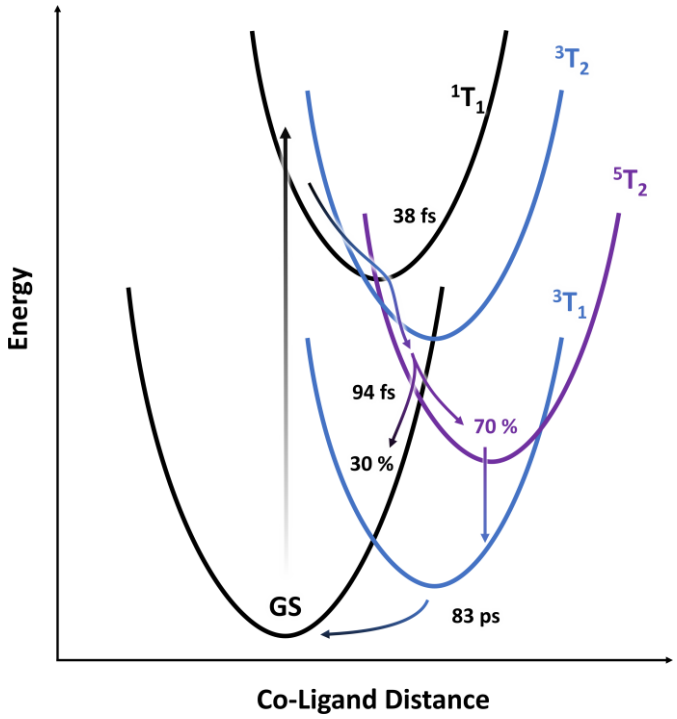

Figure 5. Schematic representing potential energy surfaces in the proposed model.

states. For example, Sousa *et al* calculated a spin-orbit coupling matrix element of up to 67 cm^{-1} for the $^1MLCT \rightarrow {}^5T_2$ crossing in $Fe(bpy)_3^{2+}$, only a factor of 3-5 less than the maximum coupling for $^3T \rightarrow {}^5T_2$ transitions. Given the ~100% quantum yield of the $^3T \rightarrow {}^5T_2$ process found in Fe(III) complexes, a 30% efficient ΔS=2 process becomes increasingly plausible. While our treatment thus far has considered all of the photophysics to occur at a single Co center, the four cobalt atoms within the cubane cluster exhibit significant electronic delocalization and metal-metal interactions,[40] which would enhance any heavy-atom effects on ISC rate.[41,42]

Further theoretical work will be required to map the excited-state potential energy surfaces and the coupling between them, though the presence of four metal centers will be a considerable computational challenge. The Co_4O_4 cubane itself presents a flexible platform for substitution of its ligands[43] and incorporation of heterometals into its core,[44] potentially providing insights into the factors affecting ultrafast ISC. We note that the high cross-section of M-edge XANES transitions results in a strong transient signal even with low excitation density (4% per cubane, 1% per Co), avoiding multiple excitation of a single cubane and simplifying the analysis.

In conclusion, time resolved M-edge XANES spectroscopy was used to probe the metal-centered dynamics of the cobalt cubane Co_4O_4 after pumping its *d-d* transitions at 550 nm. This revealed the presence of a short-lived singlet state that rapidly undergoes intersystem crossing into the quintet state within 38 fs. This quintet was identified by comparison with LFM simulations and with the M-edge XANES signal of the authentic quintet in the isoelectronic $Fe(phen)_3^{2+}$ system. Ballistic back-intersystem crossing returns 30% of the quintet to the singlet ground state in 94 fs. The remainder of the quintet progresses into a metastable triplet state which then relaxes back to the ground state in 83 ps. This work highlights the aptitude of M-edge XANES spectroscopy towards the characterization of short-lived metal-centered states in transition metal complexes, and shows that single-step ΔS=2 ISC is a viable decay pathway in such systems.

Conflicts of interest

There are no conflicts to declare.

Supporting Information

Details concerning the synthesis of cobalt cubane, sample preparation, LFM and density functional theory simulations, and the M-edge XANES spectrometer may be found in the electronic supplementary information.

Acknowledgements

This material is based upon work supported by the U.S. Department of Energy, Office of Science, Office of Basic Energy Sciences under Award Number DE-SC0018904. This material is based upon work supported by the National Science Foundation Graduate Research Fellowship under Grant No. DGE-1746047. The XUV instrument was built with partial support from the Air Force Office of Scientific Research under AFOSR Award No. FA9550-14-1-0314.

References

1 A. Genoni, G. La Ganga, A. Volpe, F. Puntoriero, M. Di Valentin, M. Bonchio, M. Natali and A. Sartorel, *Faraday Discuss.*, 2015, **185**, 121–141.
2 H. Liu and H. Frei, *ACS Catal.*, 2020, **10**, 2138–2147.
3 S. Berardi, G. La Ganga, M. Natali, I. Bazzan, F. Puntoriero, A. Sartorel, F. Scandola, S. Campagna and M. Bonchio, *J. Am. Chem. Soc.*, 2012, **134**, 11104–11107.
4 W. Jiang, X. Yang, F. Li, Q. Zhang, S. Li, H. Tong, Y. Jiang and L. Xia, *Chem. Commun.*, 2019, **55**, 1414–1417.
5 J. Li, Y. Jiang, Q. Zhang, X. Zhao, N. Li, H. Tong, X. Yang and L. Xia, *RSC Adv.*, 2017, **7**, 4102–4107.
6 B. Zhang, F. Li, F. Yu, X. Wang, X. Zhou, H. Li, Y. Jiang and L. Sun, *ACS Catal.*, 2014, **4**, 804–809.
7 Y. Wang, F. Li, X. Zhou, F. Yu, J. Du, L. Bai and L. Sun, *Angew. Chemie - Int. Ed.*, 2017, **56**, 6911–6915.
8 S. Ye, C. Ding, R. Chen, F. Fan, P. Fu, H. Yin, X. Wang, Z. Wang, P. Du and C. Li, *J. Am. Chem. Soc.*, 2018, **140**, 3250–3256.
9 O. S. Wenger, *Chem. - A Eur. J.*, 2019, **25**, 6043–6052.
10 J. K. McCusker, *Science*, 2019, **363**, 484–488.
11 J. K. McCusker, K. N. Walda, D. Magde and D. N. Hendrickson, *Inorg. Chem.*, 1993, **32**, 394–399.
12 L. Ferrari, M. Satta, A. Palma, L. Di Mario, D. Catone, P. O'Keeffe, N. Zema, T. Prosperi and S. Turchini, *Front. Chem.*, 2019, **7**, 348.
13 J. Vura-Weis, C. M. Jiang, C. Liu, H. Gao, J. M. Lucas, F. M. F. De Groot, P. Yang, A. P. Alivisatos and S. R. Leone, *J. Phys.*

Chem. Lett., 2013, **4**, 3667–3671.
14 C. M. Jiang, L. R. Baker, J. M. Lucas, J. Vura-Weis, A. P. Alivisatos and S. R. Leone, *J. Phys. Chem. C*, 2014, **118**, 22774–22784.
15 A. Cirri, J. Husek, S. Biswas and L. R. Baker, *J. Phys. Chem. C*, 2017, **121**, 15861–15869.
16 M. A. Verkamp, J. Leveillee, A. Sharma, A. Schleife and J. Vura-Weis, 2019, DOI:10.26434/chemrxiv.8323289.v1.
17 S. K. Cushing, A. Lee, I. J. Porter, L. M. Carneiro, H. T. Chang, M. Zürch and S. R. Leone, *J. Phys. Chem. C*, 2019, **123**, 3343–3352.
18 E. Principi, E. Giangrisostomi, R. Mincigrucci, M. Beye, G. Kurdi, R. Cucini, A. Gessini, F. Bencivenga and C. Masciovecchio, *Phys. Rev. B*, 2018, **97**, 174107.
19 S. K. Cushing, I. J. Porter, B. R. de Roulet, A. Lee, B. M. Marsh, S. Szoke, M. E. Vaida and S. R. Leone, *Sci. Adv.*, 2020, **6**, eaay6650.
20 E. S. Ryland, K. Zhang and J. Vura-Weis, *J. Phys. Chem. A*, 2019, **123**, 5214–5222.
21 R. Ash, K. Zhang and J. Vura-Weis, *J. Chem. Phys.*, 2019, **151**, 104201.
22 K. Zhang, R. Ash, G. S. Girolami and J. Vura-Weis, *J. Am. Chem. Soc.*, 2019, **141**, 17180–17188.
23 T. C. Davenport and T. D. Tilley, *Dalt. Trans.*, 2015, **44**, 12244–12255.
24 S. A. Chavan, D. Srinivas and P. Ratnasamy, *J. Catal.*, 2001, **204**, 409–419.
25 A. R. Riordan, A. Jansma, S. Fleischman, D. B. Green and D. R. Mulford, *Chem. Educ.*, 2005, **10**, 115–119.
26 Y. Shari'ati and J. Vura-Weis, 2021, DOI:arXiv.2108.07191.
27 K. Zhang, M. F. Lin, E. S. Ryland, M. A. Verkamp, K. Benke, F. M. F. De Groot, G. S. Girolami and J. Vura-Weis, *J. Phys. Chem. Lett.*, 2016, **7**, 3383–3387.
28 K. S. Kjær, T. B. Van Driel, T. C. B. Harlang, K. Kunnus, E. Biasin, K. Ledbetter, R. W. Hartsock, M. E. Reinhard, S. Koroidov, L. Li, M. G. Laursen, F. B. Hansen, P. Vester, M. Christensen, K. Haldrup, M. M. Nielsen, A. O. Dohn, M. I. Pápai, K. B. Møller, P. Chabera, Y. Liu, H. Tatsuno, C. Timm, M. Jarenmark, J. Uhlig, V. Sundström, K. Wärnmark, P. Persson, Z. Németh, D. S. Szemes, É. Bajnóczi, G. Vankó, R. Alonso-Mori, J. M. Glownia, S. Nelson, M. Sikorski, D. Sokaras, S. E. Canton, H. T. Lemke and K. J. Gaffney, *Chem. Sci.*, 2019, **10**, 5749–5760.
29 N. A. Miller, A. Deb, R. Alonso-Mori, J. M. Glownia, L. M. Kiefer, A. Konar, L. B. Michocki, M. Sikorski, D. L. Sofferman, S. Song, M. J. Toda, T. E. Wiley, D. Zhu, P. M. Kozlowski, K. J. Kubarych, J. E. Penner-Hahn and R. J. Sension, *J. Phys. Chem. A*, 2018, **122**, 4963–4971.
30 G. Auböck and M. Chergui, *Nat. Chem.*, 2015, **7**, 629–633.
31 S. Zerdane, M. Cammarata, O. Iasco, M. L. Boillot and E. Collet, *J. Chem. Phys.*, 2019, **151**, 171101.
32 C. Bressler, C. Milne, V.-T. Pham, A. ElNahhas, R. M. van der Veen, W. Gawelda, S. Johnson, P. Beaud, D. Grolimund, M. Kaiser, C. N. Borca, G. Ingold, R. Abela and M. Chergui, *Science*, 2009, **323**, 489–492.
33 W. Baker and M. Van Veenendaal, *Phys. Rev. B*, 2021, **104**, 014407.
34 J. Chang, A. J. Fedro and M. Van Veenendaal, *Phys. Rev. B - Condens. Matter Mater. Phys.*, 2010, **82**, 075124.
35 C. Sousa, A. Domingo and C. de Graaf, *Chem. - A Eur. J.*, 2018, **24**, 5146–5152.
36 C. Sousa, M. Llunell, A. Domingo and C. De Graaf, *Phys. Chem. Chem. Phys.*, 2018, **20**, 2351–2355.
37 M. Van Veenendaal, *Sci. Rep.*, 2017, **7**, 6672.
38 R. Chakrabarty, S. J. Bora and B. K. Das, *Inorg. Chem.*, 2007, **46**, 9450–9462.
39 A. Britz, W. Gawelda, T. A. Assefa, L. L. Jamula, J. T. Yarranton, A. Galler, D. Khakhulin, M. Diez, M. Harder, G. Doumy, A. M. March, É. Bajnóczi, Z. Németh, M. Pápai, E. Rozsályi, D. Sárosiné Szemes, H. Cho, S. Mukherjee, C. Liu, T. K. Kim, R. W. Schoenlein, S. H. Southworth, L. Young, E. Jakubikova, N. Huse, G. Vankó, C. Bressler and J. K. McCusker, *Inorg. Chem.*, 2019, **58**, 9341–9350.
40 R. G. Hadt, D. Hayes, C. N. Brodsky, A. M. Ullman, D. M. Casa, M. H. Upton, D. G. Nocera and L. X. Chen, *J. Am. Chem. Soc.*, 2016, **138**, 11017–11030.
41 C. M. Marian, *Annu. Rev. Phys. Chem.*, 2020, **72**, 617–640.
42 Y. Shimizu and T. Azumi, *J. Phys. Chem.*, 1982, **86**, 22–26.
43 A. I. Nguyen, J. Wang, D. S. Levine, M. S. Ziegler and T. D. Tilley, *Chem. Sci.*, 2017, **8**, 4274–4284.
44 A. I. Nguyen, D. L. M. Suess, L. E. Darago, P. H. Oyala, D. S. Levine, M. S. Ziegler, R. D. Britt and T. D. Tilley, *J. Am. Chem. Soc.*, 2017, **139**, 5579–5587.